Dynamical principles of cell-cycle arrest: Reversible, irreversible, and mixed strategies

Benjamin Pfeuty*

Laboratoire de Physique des Lasers, Atomes, et Molécules, Centre National de la Recherche Scientifique, UMR 8523, Université Lille 1, F-59655 Villeneuve d'Ascq, France

(Received 26 May 2012; revised manuscript received 25 July 2012; published 21 August 2012)

Living cells often alternate between proliferating and nonproliferating states as part of individual or collective strategies to adapt to complex and changing environments. To this aim, they have evolved a biochemical regulatory network enabling them to switch between cell-division cycles (i.e., oscillatory state) and cell-cycle arrests (i.e., steady state) in response to extracellular cues. This can be achieved by means of a variety of bifurcation mechanisms that potentially give rise to qualitatively distinct cell-cycle arrest properties. In this paper, we study the dynamics of a minimal biochemical network model in which a cell-division oscillator and a differentiation switch mutually antagonize. We identify the existence of three biologically plausible bifurcation scenarios organized around a codimension-four swallowtail-homoclinic singularity. As a result, the model exhibits a broad repertoire of cell-cycle arrest properties in terms of reversibility of these arrests, tunability of interdivision time, and ability to track time-varying signals. This dynamic versatility would explain the diversity of cell-cycle arrest strategies developed in different living species and functional contexts.

DOI: 10.1103/PhysRevE.86.021917 PACS number(s): 87.16.Yc, 87.17.Aa, 87.17.Ee, 87.18.Cf

I. INTRODUCTION

Switching behaviors between cyclic and steady states occur in many physical, chemical, and biological systems [1,2]. The nature of the underlying dynamic mechanisms can be remarkably diverse [3], depending on the detailed structural properties of the system. This is especially the case in biological systems in which evolution or adaptation can tune biophysical processes to achieve a specific biological function. For instance, the mechanisms bringing neurons from resting to spiking states rely on various types of bifurcation depending on the detailed ionic current properties [4], which account for the neuronal diversity of firing patterns [5,6] or synchronization ability [7]. Which bifurcation mechanisms give rise to oscillations also determine important properties of oscillatory signaling pathways in living cells [8–11].

The cell-division cycle is another, and perhaps the most vital, biological process that is driven by a biochemical oscillator [12], which can be nevertheless stopped under some circumstances [Fig. 1(a)]. On the one hand, the cyclic alternation of phases of growth and division underlies cellular proliferation that is essential for the colonization of environmental niches or the development of multicellular organisms. On the other hand, specific environmental signals, such as stress factors, may stop this cycling process, allowing cells to wait for better conditions or to enter into a specialized state during which they may repair damages, adopt survival strategies, or contribute to the division of labor in cell societies. The process by which cells stop their progression through the cell-division cycle and eventually diverge toward another fate is called cell-cycle arrest (or exit) and may follow various decision-making rules depending on the cellular context. For instances, some nondividing cells retain the ability to resume their cell-division cycle when the antimitogenic signal vanishes [13,14], whereas others lose partially or fully their proliferative capacity [15,16]. Noteworthily, irreversible commitment often takes place after a precommitment stage during which cells can quickly reenter into the cell cycle [17,18].

The goal of this paper is to identify the main design and dynamical principles that account for such a diversity of cell-cycle arrest strategies used by cells to switch between proliferating and nonproliferating states. Modeling approaches have provided a comprehensive picture of the generic mechanisms of growth-dependent cell-cycle progression in eukaryotic cells [19]. Basically, the cell-cycle regulatory network features several positive and negative feedback loops that drive a cyclic sequence of states separated by irreversible transitions [20]. Recent modeling studies have complemented this picture by taking into account some specific stress or differentiation signaling pathways that counteract cell division [21–23]. It was shown that both the intrinsic dynamics of these signaling modules and their coupling properties to the cell-division machinery play an important role in determining the manner in which the cell-cycle progression would slow down or arrest, reversibly or irreversibly, in response to these antiproliferative ansignals. These models are nevertheless based on signaling and regulatory features that are specific to a given living species or extracellular context. In contrast, the approach undertaken in this study seeks to represent the generic dynamics of the cell-cycle arrest process with a minimal mathematical model involving a small set of variables and parameters of biological significance. The preliminary part of this study will be devoted to design such a model of cell-cycle arrest based on the coupling between two modules: a cell-cycle oscillator and a differentiation switch. The bifurcation analysis of the model will help us to identify the different dynamical regimes through which cells may arrest their cell-division cycle and the key control parameters in this process. Finally, emphasis will be put on the diversity of functional properties, such as frequency tunability or response to time-varying signals, that are deployed in these different dynamical regimes.

*benjamin.pfeuty@univ-lille1.fr

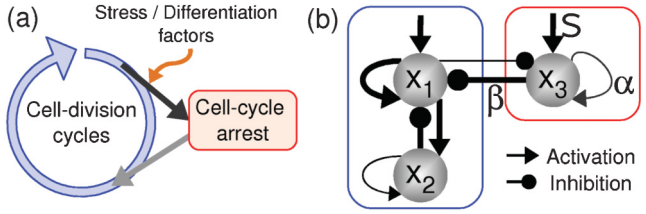

(c)

Cell-cycle arrest	x_1	x_3	Refs
Bacterial SOS response	FtsZ	SulA	[41]
Bacillus competence	FtsW	Maf	[42]
Yeast mating	Cln1-3	Far1	[43]
Yeast osmotic stress response	Clb5,6 / Cln1-2	Hog1 / Sic1	[22]
Plant stress response	Cyclin -CDKA	KRP	[44]
Plant DNA stress response	Cyclin B-CDKA/B	Wee1	[45]
Drosophila differentiation	Cyclin E-Cdk2	Dacapo	[46]
Mammalian quiescence	Cyclin D/E-Cdk2/4	Rb	[47]
Mammalian differentiation	Cyclin E-Cdk2	Cip / Kip	[48]
Animal ovocyte G2 arrest	Cyclin B-Cdk1	Myt1	[49]

FIG. 1. (Color online) (a) Schematic representation of the biological process of cell-cycle arrest and reentry. (b) Generic biochemical network model of cell-cycle arrest where thick and thin arrows indicate mandatory and optional links for cell-cycle arrest. (c) Examples of antagonistic interactions (x_3 inhibits x_1 and reciprocally in most cases) involved in cell-cycle arrest in bacteria [41,42], plants [44,45], yeast [22,43], and animals [46–49].

II. MINIMAL NETWORK MODEL OF CELL-CYCLE ARREST

A. Network component dynamics

The cell-cycle biochemical network involves the interactions between a large number of proteins including transcriptional activators and repressors as well as kinases and kinase-regulatory proteins, which altogether interact at different regulatory levels: transcription, degradation, phosphorylation, multimerization, or sequestration. Very simple models have nevertheless been proven useful to capture some key qualitative features of the cell-division cycle [24–26]. We consider here a minimal network model that gives greater importance to the network architecture rather than to the detailed reaction rate equations. Thus, we assume that the normalized concentration of a given active protein i evolves in time according to the following generic dynamic equation (see Appendix):

$$\tau_i \frac{dx_i}{dt} = \left(s_i + \sum_j a_{ij} x_j^2\right)(1 - x_i) - \left(d_i + \sum_j b_{ij} x_j^2\right) x_i, \tag{1}$$

where the first and second members are the activating and inactivating kinetic rates, which may both depend on the concentrations of other active proteins j. This dynamical system is characterized by a bounded phase space ($x \in [0,1]$), which is due to inherent saturation effects in biochemical reactions. In this study, basal inactivation rates d_i are set to 1 upon parameter renormalization. Note that for a single self-activating component, a cusp singularity can be found for the following coordinates: $x_c = 1/3$, $a_c = 3.375$, $s_c = 1/8$. It means that the self-activating component behaves as a bistable switch for $a_{ii} > a_c$.

B. Network topology and control parameters

We consider a minimal network topology having solely three types of regulatory proteins [Fig. 1(b)]: Proteins 1 and 2 regulate the division cycle in which the first protein (e.g., cyclin-CDK in eukaryotic cells) activates and is inactivated by the second protein (e.g., APC in eukaryotic cells). Moreover, these two proteins are considered to be self-activating ($a_{1,2} > a_c$), owing to fast positive feedback mechanisms that contribute to sharp, eventually bistable, responses. Protein 3 is an inhibitor of cell division that inactivates the cell-cycle activator (protein 1). This inhibition is a hallmark of most cases of cell-cycle arrest occurring in various organisms and contexts [Fig. 1(c)]. A frequent property of such cell-cycle antagonist is to be inhibited, in turn, by cell-cycle activators, here protein 1, and to be part of a module that may involve positive feedback mechanisms. The activation and inactivation matrices associated with this minimal topology are then given by

$$a_{ij} = \begin{pmatrix} a_{11} & 0 & 0 \\ a_{21} & a_{22} & 0 \\ 0 & 0 & \underline{\alpha} \end{pmatrix} \quad b_{ij} = \begin{pmatrix} 0 & b_{12} & \underline{\beta} \\ 0 & 0 & 0 \\ b_{31} & 0 & 0 \end{pmatrix}.$$

The main signals that control this network are those that activate the positive regulator of cell division (i.e., growth factors) and those that activate the regulator that antagonizes with cell division (i.e., stress or differentiation factors), so that we can write the input vector as

$$s_i = (s_1\ 0\ \underline{S}).$$

Underlined parameters α, β, and S are the main control parameters that are actually varied in the course of our model analysis.

III. BIFURCATION THEORY OF CELL-CYCLE ARREST

A. Distinct scenarios of cell-cycle arrest

In the absence of the stress/differentiation signal ($S = 0$ and $x_3 = 0$), the model reduces to a two-dimensional system in which a core negative feedback loop contributes to stable limit cycle oscillations in some domain of the parameter space. In this study, parameters are set to $a_{11} = 5$, $a_{22} = 3.8$, $b_{12} = 4$, $a_{21} = 4$, $\tau_1 = 1$, $\tau_2 = 0.5$, and $s_1 = 0.1$. These model parameters lead to oscillations occurring at frequency $f_0 = 0.035$. Both the choice of τ_1 and τ_2 of the same order and the choice of a_{11} and a_{22} sufficiently large ($> a_c$) contributes to the existence of large amplitude oscillations that typically appear or disappear through a saddle-node bifurcation on an invariant circle (SNIC) under smooth changes of the signal s_1.

In the presence of the stress/differentiation signal S, the stable limit-cycle oscillation disappears for a certain critical values S^* of S. We found that such disappearance occurs via several main bifurcation routes [Fig. 2], depending on the precise value of some key parameters of the differentiation module (α, β, b_{31}):

(i) *$SNIC_0$ scenario.* For sufficiently small values of α (including the case $\alpha = 0$), x_3 varies smoothly with S, then the disappearance of stable oscillations occurs through a SNIC bifurcation [Fig. 2(a)]. In this bifurcation regime, cell-cycle arrest is fully reversible as oscillations resume for S decreasing

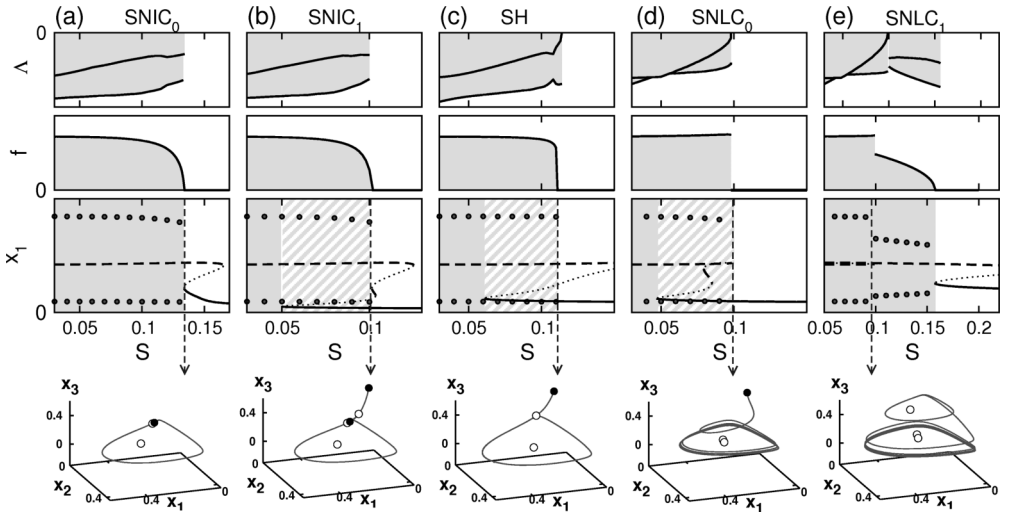

FIG. 2. Main bifurcation scenarios for cell-cycle arrest. In the three top panels, plots of the two negative Floquet exponents Λ, the oscillation frequency f, and the underlying bifurcation diagrams as functions of S. In the bifurcation diagrams: full (dashed) lines indicate stable (unstable) fixed point; circles indicate the maximal and minimal x_1 values during oscillation; white and gray domains indicate the existence of a stable steady state and a stable limit cycle, respectively. In the bottom panels, plots of trajectories (gray lines) and fixed point (stable/unstable: filled/empty circles) in the phase space at the bifurcation point ($S = S^*$). Left to right panels correspond to different sets of model parameters associated with distinct bifurcation scenarios: (a) SNIC_0 scenario ($\alpha = 3.2$, $\beta = 5$, $b_{31} = 2$): Occurrence of a saddle-node bifurcation on an invariant circle. (b) SNIC_1 scenario ($\alpha = 3.8$, $\beta = 8$, $b_{31} = 2$): Sequential occurrences of two saddle-node bifurcations, off and on an invariant circle. (c) SH scenario ($\alpha = 3.8$, $\beta = 2$, $b_{31} = 2$): Sequential occurrences of a saddle-node bifurcation off an invariant circle and a saddle-homoclinic bifurcation. (d) SNLC_0 scenario ($\alpha = 3.8$, $\beta = 2$, $b_{31} = 0$): Occurrence of a saddle-node bifurcation of two limit cycles. (e) SNLC_1 scenario ($\alpha = 3.8$, $\beta = 0.5$, $b_{31} = 0$): Sequential occurrence of a saddle-node bifurcation of two limit cycles and a SNIC_0 bifurcation.

below S^* and the frequency of oscillation scales as $\sqrt{S^* - S}$ as the bifurcation parameter approaches S^*.

(ii) *SNIC_1 scenario*. For sufficiently large values of α and β, the SNIC bifurcation point coexists with another stable steady state. As a result, hysteretic behavior occurs when increasing S switches the system to this alternative state through a saddle-node bifurcation at $S = S_{c1} > S^*$, whereas further decrease of S destabilizes this state through a saddle-node bifurcation *off* an invariant circle at $S = S_{c2} < S^*$ [Fig. 2(b)].

(iii) *SH scenario*. Besides the two SNIC bifurcation scenarios above, the limit-cycle oscillations can also disappear through a collision with a hyperbolic saddle equilibria, which is usually called a saddle homoclinic (SH) bifurcation. Close to the bifurcation point, the limit cycle approaches the saddle equilibria in a way that the oscillation frequency scales as $1/\ln(S^* - S)$. It is to note that this scenario is always associated with a hysteretic behavior when increasing and then decreasing the bifurcation parameter S [Fig. 2(c)].

(iv) *SNLC scenarios*. At last, two others scenarios, occurring for small values of b_{31} and high values of α, involve a saddle-node bifurcation of limit cycles (SNLC). In this bifurcation scenario, a stable limit cycle coalesces with a saddle one, so that trajectories further converge to either a fixed point (SNLC_0) [Fig. 2(d)] or another limit cycle (SNLC_1) [Fig. 2(e)]. The SNLC_0 case is characterized by a hysteretic behavior and a finite frequency at the bifurcation point. In contrast with previous scenarios, cell-cycle exit may occur at any phase of the cell-cycle oscillation, which is very unlikely from a biological perspective for which such exit is restricted to specific phases of the cell-division cycle. The SNLC_1 case displays discrete changes of both amplitude and frequency of cell-cycle oscillation upon change of the stress/differentiation signal, which is also biologically irrelevant.

B. Unfolding of a swallowtail-homoclinic bifurcation

The three biologically plausible types of the codimension-one bifurcation scenario depicted above (SNIC_0, SNIC_1, SH) occur in well-defined domains of the parameter space with coordinates α, β, S, and τ_3. In this four-dimensional parameter space, these domains intersect into a single point ($\tilde{\alpha}$, $\tilde{\beta}$, $\tilde{S}$, $\tilde{\tau}_3$) where a codimension-four bifurcation occurs: the limit cycle collides with a swallowtail singularity. Close to this singularity, the present model can be reduced by means of appropriate changes of coordinates to the truncated normal form given by the three-parameter family of vector fields [27],

$$\begin{aligned} z_1' &= -z_1 \\ z_2' &= -z_2 \\ z_3' &= r_1 + r_2 z_3 + r_3 z_3^2 - z_3^4, \end{aligned} \tag{2}$$

where $r_{1,2,3}(\tilde{\alpha}, \tilde{\beta}, \tilde{S}) = 0$. The condition for the homoclinic connection to this swallowtail fixed point occurs for $\tau_3 = \tilde{\tau}_3$. A swallowtail-homoclinic bifurcation requires then four parameters to completely unfold it into n-dimensional manifolds of codimension-$(4 - n)$ bifurcations ($1 \leqslant n \leqslant 3$).

Figure 3(a) shows a two-dimensional section [$\tau_3 = \tilde{\tau}_3$ and $S = S^*(\alpha, \beta, \tau_3)$] of this parameter space where SH, SNIC_0, and SNIC_1 domains intersect into lines on which codimension-two bifurcation occurs: (i) a saddle-node homoclinic bifurcation (line II in Fig. 3); (ii) two saddle-node bifurcations, *off* and *on* an invariant circle (line III in Fig. 3); (iii) a saddle-node bifurcation on a homoclinic connection (line IV in

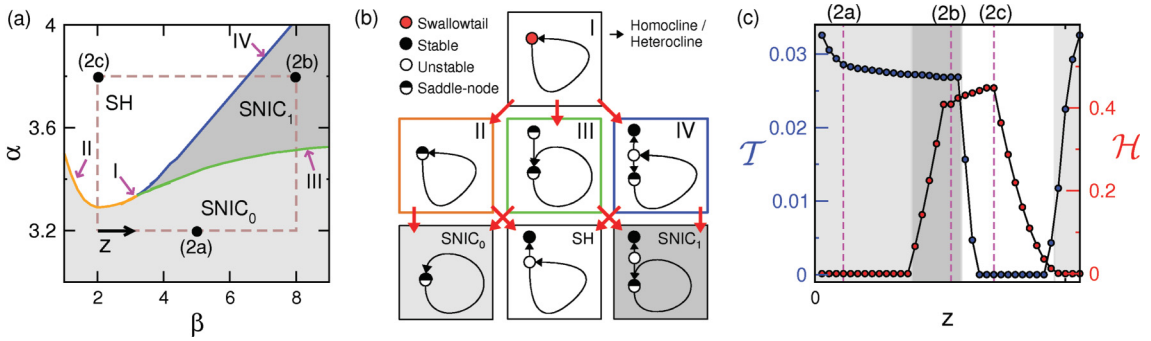

FIG. 3. (Color online) (a) Phase diagram as a function of α and β for $\tau_3 = 0.78$, $b_{31} = 2$, and $S = S^*(\alpha,\beta)$. Dashed line indicates the path used for the panel (c) and black circles indicate parameters used in Fig. 2. (b) Schematic phase portrait of various bifurcation scenarios of codimension one (bottom), two (middle), and four (top). (c) The frequency tunability ($\mathcal{T}$) and the hysteresis width ($\mathcal{H}$) as a function of the z coordinate along the path drawn in the phase diagram (a). In (a)–(c), grayscale indicates SNIC bifurcation scenarios (light gray: $SNIC_0$; dark gray: $SNIC_1$)

Fig. 3). These lines finally intersect into the codimension-four swallowtail-homoclinic singularity. If τ_3 varies, these lines do not intersect anymore into one point and a more complex phase diagram with several codimension-three singularities appears in the vicinity of the swallowtail-homoclinic singularity.

Operating close to this codimension-four singularity provides the biochemical network with the ability to deploy very different properties of cell-cycle arrest and reentry upon slight changes of parameters. This is shown by defining a path in the parameter space that encloses this singularity [Fig. 3(a)] and by measuring two quantities along this path [Fig. 3(c)]: (i) the hysteresis size $\mathcal{H}$ defined as $(S^* - S^+)/S^*$ where S^+ is the signal level for which oscillations appear when decreasing S; (ii) the frequency tunability $\mathcal{T}$ is defined as $(S^* - S^{50\%})/S^*$ where $f(S^{50\%}) = 0.5\, f_0$. Figure 3(c) shows that both quantities vary relatively independently depending on the bifurcation scenario. The $SNIC_0$ bifurcation scenario exhibits both fully reversible arrest ($\mathcal{H} = 0$) and frequency tunability. In sharp contrast, the SH bifurcation scenario is characterized by hysteretic behavior of various extents combined with a lack of frequency tunability ($\mathcal{T} = 0$), which is consistent with the fact that the period of the oscillation approaches infinity logarithmically in this scenario. Alternatively, frequency tunability coexists with hysteretic behavior in the $SNIC_1$ bifurcation scenario whereas the opposite occurs at the border between the SH and $SNIC_0$ bifurcation scenarios. Thus, several patterns of combined properties of hysteretic size and frequency tunability can be achieved upon moderate changes of model parameters, which is likely to be useful for the adaptive or evolutionary selection of an optimal cell-cycle arrest strategy.

C. Response to time-varying signals

The switching events between proliferating and nonproliferating states occurs upon temporal variations of division, stress, and differentiation signals. These variations can occur over a wide range of timescales that can be either larger or smaller than the cell-cycle period. How do cells interpret these time-varying signals and divide or exit from their cell cycle accordingly? A hypothesis is that, like other properties of cell-cycle arrest, it depends critically on the underlying bifurcation scenario. To check this hypothesis, we perform numerical simulations of the network dynamics in response to a periodic signal of fixed mean S_m, but variable frequency f and amplitude A

$$S(t) = S_m[1 + A\, cos(2\pi\ f\ t)]. \tag{3}$$

The value of S_m is chosen to be slightly lower than the critical value S^*: $S^m = S^* - \eta$ with $\eta = 0.03$. We measure the values $S_i^* = S(t_i^*)$ where t_i^* is the time of division (i.e., corresponding to the maximum value of x_1), such as to define a normalized quantity χ,

$$\chi = \frac{S_m - \langle S^* \rangle}{A}. \tag{4}$$

χ equal to 1 (-1) indicates that division events are fully anticorrelated (correlated) with the stress/differentiation signal.

Figure 4 compares the response to this time-varying input for the three classes of models in which $SNIC_0$, $SNIC_1$, and SH bifurcations occur, respectively [same parameters as in Figs. 2(a)–2(c)]. Both similarities and discrepancies are observed. On the one hand, all models display a 1:1 synchronization tongue shown in Fig. 4(a) that connects to the natural frequency f_0 at vanishing amplitude of signal oscillation. This synchronization region correlates with values of χ close to 1 [Fig. 4(b)], which indicate a high anticorrelation between division event and the stress/differentiation signal. On the other hand, this region of 1:1 synchronization and of high values of χ is found to be much larger in the case of the $SNIC_0$ or $SNIC_1$ bifurcation scenarios than in that of SH bifurcation scenario, although the $SNIC_1$ and SH scenarios display hysteresis of similar extent.

These qualitatively different synchronization properties are related with the distinct manner by which the phase-space trajectory converges to the steady state for suprathreshold signal ($S > S^*$). In the $SNIC_0$ bifurcation scenario, the transverse stability of the whole trajectory contributes to the stabilization of the 1:1 synchronization state. In addition, the proximity in phase space between the stable steady state and the limit cycle allows to keep the convergence time (to the steady state) small enough. As a result, the system is reset for a large range of forcing frequency to the same state before resuming cell-cycle oscillations. This is in stark contrast with what happens in the SH bifurcation scenario: transverse instability can occur

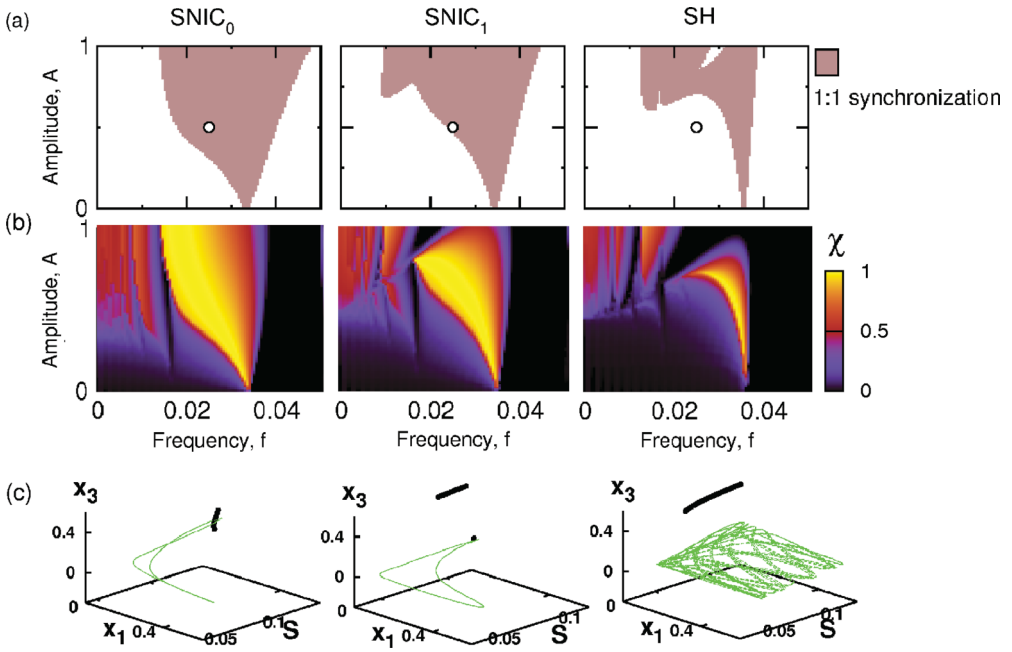

FIG. 4. (Color online) Dynamic response to a sinusoidal signal $S(t)$ [see Eq. (3)] in the different bifurcation scenarios [Left: $SNIC_0$ with the same parameters as in Fig. 2(a); Middle: $SNIC_1$ with the same parameters as in Fig. 2(b); Right: SH with the same parameters as in Fig. 2(c)]. (a)–(b) Plots of the 1:1 synchronization region (a) and χ (b) as a function of the frequency f and amplitude A of the signal. (c) Plots of the phase-space trajectories (thin green line) relative to the position of the steady-state solution branch (thick black line) for a given signal modulation [circles in (a): $f = 0.025$ and $A = 0.5$].

when the trajectory crosses a homoclinic manifold (for a given value of S) and the convergence time is typically large due to the discrete distance in phase space between the limit cycle and the stable steady state. These arguments are schematically illustrated in Fig. 4(c) where it is shown that the phase-space trajectory approaches one steady-state branch in the $SNIC_0$ and $SNIC_1$ scenarios, in which synchronization occurs, but not in the SH scenario. Interestingly also, the existence of two steady-state branches provides the $SNIC_1$ model with the ability to elicit hysteretic responses when the signal changes slowly enough but fully reversible responses with prompt reentry into the cell-division cycle when the signal changes at the typical timescale of the cell-division period.

IV. CONCLUSION

In summary, we have shown that the properties of cell-cycle arrest are tightly related with the underlying bifurcation scenario that itself depends on a few key network features. In particular, the self-activating or inhibitory strengths of the antiproliferative pathway critically determine the manner in which cell-cycle oscillations slow down, stop, restart, and synchronize in response to time-varying signals. The experimental assessment of these design principles would be to determine how genetic or pharmacological perturbations of cell-cycle inhibitory components impact cell-cycle arrest properties in response to various stress protocols. Whatever the type of stress (thermal, oxidative, osmotic, nutrient deprivation, etc.), the important point is to expose cells to temporal patterns of stress such as oscillations of various frequencies, to allow the estimation of the extent of both hysteresis and synchronization. The identification of several biologically plausible bifurcation scenarios provides also a comprehensive picture that encompasses the distinct cell-cycle arrest strategies encountered in different species or contexts. On the one hand, the $SNIC_0$ bifurcation scenario corresponds to the reversible arrest strategy in which cells promptly resume their division cycle upon removal of the stress or differentiation signal. On the other hand, the SH bifurcation scenario fits with the irreversible differentiation strategy required to withdraw from the cell division for some period of time or permanently, such as in terminal differentiation or senescence. Interestingly, the $SNIC_1$ bifurcation scenario provides a mixed strategy that combines irreversible arrest for slow and significant changes in the signal and reversible arrest for rapid or moderate changes in the signal. Several cell-cycle arrest processes in bacteria, amoebae, or mammals [17,18,28,29] seem to follow this scheme in which a reversible step precedes an irreversible decision. Consistent with our study, this hybrid strategy has been proposed to maximize both adaptable and reliable decision making over a broad range of dynamic environmental changes [29]. It also provides a simple mechanism to account for the lengthening of the G1 phase observed during animal development that precedes irreversible differentiation of stem and progenitor cells [30].

Our study also sheds light on another important aspect of cell division control, which is the periodic forcing of the cell-cycle oscillator [31]. The *in vivo* origin of this modulation can be the 24-hour periodic circadian gating associated with day-night alternation [32] or the ultradian oscillations in signaling pathways [33,34]. The ability for the cell-division cycle to be entrained for a large range of forcing frequency and amplitude may provide some selective advantage to cells in these specific contexts. Likewise, a large 1:1 synchronization domain has

been shown to be important for the robust entrainment of circadian oscillators [35] or for the reliability of neuronal firing [36].

More generally, this study stresses the fact that biological systems are likely to harness the dynamical versatility and flexibility in the vicinity of high-codimension singularities, as it has also been shown in other biochemical circuit designs [37–40]. A further step will be to delineate how slower adaptive or evolutionary forces drive these systems to select appropriate dynamical behaviors in a context-dependent manner, which is a key property of living systems.

APPENDIX

In this appendix we describe in some detail the generic mathematical form used in Eq. (1) to represent the time evolution of protein concentrations. Such dynamic evolution can be controlled at various levels such as by phosphorylation/dephosphorylation mechanisms, transcriptional control or degradation.

Let consider first the case in which the activity of proteins $\mathcal{P}$ is only regulated through phosphorylation and dephosphorylation reactions, which are activating and inactivating, respectively. The reaction scheme for this system is as follows:

$$\mathcal{P} \underset{k_-}{\overset{k_+}{\rightleftharpoons}} \mathcal{P}^*, \tag{A1}$$

where the asterisk indicates the inactivated state of the protein. Defining $\tilde{x}$ and $\tilde{x}_{\rm tot}$ as the activated and total protein concentrations (in the limit of large protein number) and using the law of mass action leads to the following dynamic equation:

$$\frac{d\tilde{x}}{dt} = k_+(\tilde{x}_{\rm tot} - \tilde{x}) - k_-\tilde{x}. \tag{A2}$$

Equation (1) is finally derived after (i) normalizing the protein concentration $x = \tilde{x}/\tilde{x}_{\rm tot}$, (ii) assuming that the phosphorylation and dephosphorylation rates are the sum of a basal term and a term that depends on the concentrations of other proteins in a quadratic manner due to cooperative effects, and (iii) factorizing by the basal inactivating parameter allowing to introduce the variable τ on the left-hand side of Eq. (1).

Equation (1) is also a suitable approximation in the case of a protein species whose concentration X is regulated at the level of transcriptional activation and repression. Let us assume the existence of two classes of transcriptional factors, an inducer Y and a repressor Z, which both bound to the free promoter D encoding the regulated protein species. The inducer-promoter complex D_i (the repressor-promoter complex D_r) activates (inhibits) the transcription of mRNA. The system of reaction is given by

$$\begin{aligned} D + nY &\underset{k_-}{\overset{k_+}{\rightleftharpoons}} D_i \\ D + n'Z &\underset{K_-}{\overset{K_+}{\rightleftharpoons}} D_r \\ D_i &\overset{s_m}{\longrightarrow} D_i + \text{mRNA} \\ \text{mRNA} &\overset{d_m}{\longrightarrow} \varnothing \\ \text{mRNA} &\overset{s_P}{\longrightarrow} \mathcal{P} \\ \mathcal{P} &\overset{d_P}{\longrightarrow} \varnothing \end{aligned} \tag{A3}$$

repressor-promoter DNA complex.

Given a constant promoter concentration $D + D_i + D_r = D_{\rm tot}$ (normalized here to 1), averaging over many fast binding and unbinding events between the promoter and the transcription factors allows the computation of the mean concentration over time of the bound promoter. For sufficiently slow degradation of proteins as compared to mRNA, a quasi-steady-state approximation can be used to compute the steady-state concentration of mRNA, such that the equation for the time evolution of protein concentrations X reads

$$\frac{dX}{dt} = \frac{s_P\, s_m}{d_m} \frac{k\, Y^n}{1 + k\, Y^n + K\, Z^{n'}} - d_P X, \tag{A4}$$

where $k = k_+/k_-$ and $K = K_+/K_-$. This equation can be put into the form $\tau\,(f_1 + f_2)\,\dot{x} = f_1\,(1 - x) - f_2\,x$ after suitable renormalization: $\lambda = \frac{d_P\, d_m}{s_P\, s_m}$, $x = \lambda\, X$, and $\tau = 1/d_P$. Equation (1) can be finally obtained under the rough approximation that the quantity $f_1 + f_2$ does not vary much in the phase space.

Thus, the model using Eq. (1) implicitly omits the case of cross-regulatory events where different enzymes or different transcription factors interfere, as well as the case of regulatory schemes combining transcriptional and post-translational controls. Use of quadratic terms for transcriptional or post-translational protein interactions reflects the effect of biochemical cooperativity, providing here a primary source of nonlinearities in the model.

[1] A. Pacault, Q. Ouyang, and P. Kepper, J. Stat. Phys. **48**, 1005 (1987)

[2] J. J. Tyson, R. Albert, A. Goldbeter, P. Ruoff, and J. Sible, J. R. Soc. Interface **5**, S1 (2008).

[3] J. Guckenheimer and P. Holmes, *Nonlinear Oscillations, Dynamical Systems, and Bifurcations of Vector Fields* (Springer-Verlag, New York, 1983).

[4] M. Izhikevich, *Dynamical Systems in Neuroscience: The Geometry of Excitability and Bursting* (MIT, Cambridge, Massachusetts, 2006).

[5] D. Golomb, K. Donner, L. Shacham, D. Shlosberg, Y. Amitai, and D. Hansel, PLoS Comput. Biol. **3**, e156 (2007).

[6] S. A. Prescott, Y. D. Koninck, and T. J. Sejnowski, PLoS Comput. Biol. **4**, e1000198 (2008).

[7] R. M. Smeal, G. B. Ermentrout, and J. A. White, Philos. Trans. R. Soc. B **365**, 2407 (2010).

[8] R. Guantes and J. F. Poyatos, PLoS Comput. Biol. **2**, e30 (2006).

[9] S. Schuster, M. Marhl, and T. Hofer, Eur. J. Biochem. **269**, 1333 (2002).

[10] B. Hat, K. Puszynski, and T. Lipniacki, IET Syst. Biol. **3**, 342 (2009).

[11] X. Zhang, F. Liu, and W. Wang, Proc. Natl. Acad. Sci. USA **108**, 8990 (2011).

[12] J. E. Ferrell, T. Y. Tsai, and Q. Yang, Cell **144**, 874 (2012).

[13] S. P. Linke, K. C. Clarkin, A. D. Leonardo, A. Tsou, and G. M. Wahl, Genes Dev. **10**, 934 (1996).
[14] L. Sang, H. Coller, and J. Roberts, Science **321**, 1095 (2008).
[15] A. Takahashi, N. Ohtani, K. Yamakoshi, S. Iida, H. Tahara, K. Nakayama, K. Nakayama, T. Ide, H. Saya, and E. Hara, Nature Cell Biol. **8**, 1291 (2006).
[16] G. D. Falco, F. Comes, and C. Simone, Oncogene **25**, 5244 (2006).
[17] R. M. El-Shehawy and D. Kleiner, Phys. Plant. **119**, 49 (2003).
[18] M. Katoh, G. Chen, E. Roberge, G. Shaulsky, and A. Kuspa, Eukaryot. Cell **6**, 2038 (2007).
[19] A. Csikász-Nagy, D. Battagtokh, K. C. Chen, B. Novák, and J. J. Tyson, Biophys. J. **90**, 4361 (2006).
[20] B. Novák, J. J. Tyson, B. Gyorffy, and A. Csikász-Nagy, Nature Cell Biol. **9**, 724 (2007).
[21] J. E. Toettcher, A. Loewer, G. J. Ostheimer, M. B. Yaffe, B. Tidor, and G. Lahav, Proc. Natl. Acad. Sci. USA **106**, 785 (2009).
[22] M. A. Adrover, Z. Zi, A. Duch, J. Schaber, A. González-Novo, J. Jimenez, M. Nadal-Ribelles, J. Clotet, E. Klipp, and F. Posas, Sci. Signal **4**, ra63 (2011).
[23] B. Pfeuty, PLoS One **7**, e35291 (2012).
[24] J. R. Pomerening, E. D. Sontag, and J. E. Ferrell, Nature Cell Biol. **5**, 346 (2003).
[25] B. Pfeuty and K. Kaneko, Phys. Biol. **4**, 194 (2007).
[26] A. Csikász-Nagy, B. Novák, and J. Tyson, Adv. Exp. Med. Biol. **641**, 88 (2008).
[27] L. Perko, *Differential Equations and Dynamical Systems* (Springer-Verlag, New York, 1996).
[28] A. Skirycz, H. Claeys, S. D. Bodt, A. Oikawa, S. Shinoda, M. Andriankaja, and K. Maleux, Plant Cell **23**, 1876 (2011).
[29] A. Kuchina, L. Espinar, J. Garcia-Ojalvo, and G. M. Suel, PLoS Comput. Biol. **7**, e1002273 (2011).
[30] C. Lange and F. Calegari, Cell Cycle **9**, 1893 (2010).
[31] G. Charvin, F. Cross, and E. Siggia, Proc. Natl. Acad. Sci. USA **106**, 6632 (2009).
[32] Q. Yang, B. Pando, G. Dong, S. Golden, and A. van Oudenaarden, Science **327**, 15226 (2010).
[33] B. Mengel, A. Hunziker, L. Pedersen, A. Trusina, M. Jensen, and S. Krishna, Curr. Opin. Genet. Dev. **20**, 654 (2010).
[34] T. Kobayashi and R. Kageyama, Genes **2**, 219 (2011).
[35] B. Pfeuty, Q. Thommen, and M. Lefranc, Biophys. J. **100**, 2557 (2011).
[36] U. Beierholm, C. D. Nielsen, J. Ryge, P. Alstrom, and O. Kiehn, J. Neurophysiol. **86**, 1858 (2001).
[37] H. Song, P. Smolen, E. Av-Ron, D. A. Baxter, and J. Byrne, Biophys. J. **02**, 3407 (2007).
[38] R. Guantes and J. F. Poyatos, PLoS Comput. Biol. **4**, e1000235 (2008).
[39] B. Pfeuty and K. Kaneko, Phys. Biol. **6**, 046013 (2009).
[40] P. Rué and J. Garcia-Ojalvo, Math Biosci. **231**, 90 (2011).
[41] E. Bi and J. Lutkenhaus, J. Bacteriol. **175**, 1118 (1993).
[42] K. Briley, P. Prepiak, M. J. Dias, J. Hahn, and D. Dubnau, Mol. Microbiol. (2011).
[43] J. D. McKinney and F. R. Cross, Mol. Cell Biol. **15**, 2509 (1995).
[44] A. Verkest, C. Weinl, D. Inze, L. Veylderm, and A. Schnittger, Plant Physiol. **139**, 1099 (2005).
[45] K. De Schutter, J. Joubes, T. Cools, A. Verkest, F. Corellou, E. Babiychuk, E. Van Der Schueren, T. Beeckman, S. Kushnir, D. Inze, and L. De Veylder, Plant Cell **19**, 211 (2007).
[46] M. E. Lane, K. Sauer, K. Wallace, Y. N. Jan, C. F. Lehner, and H. Vaessin, Cell **87**, 1225 (1996).
[47] N. S. Thomas, L. C. Burke, A. Bybee, and D. C. Linch, Oncogene **6**, 317 (1991).
[48] R. A. Steinman, B. Hoffman, A. Iro, C. Guillouf, and D. A. Liebermann, Oncogene **9**, 3389 (1994).
[49] N. Nakajo, S. Yoshitome, J. Iwashita, M. Iida, K. Uto, S. Ueno, L. Okamoto, and N. Sagata, Genes Dev. **14**, 328 (2000).